Available online at www.eccomasproceedia.org
Eccomas Proceedia COMPDYN (2021) 2170-2184

ECCOMAS
Proceedia

COMPDYN 2021
8th ECCOMAS Thematic Conference on
Computational Methods in Structural Dynamics and Earthquake Engineering
M. Papadrakakis, M. Fragiadakis (eds.)
Streamed from Athens, Greece, 28 - 30 June 2021

INFLUENCE OF BEAM-TO-COLUMN CONNECTIONS IN SEISMIC VULNERABILITY ASSESSMENT OF STEEL STRUCTURES

G. Gabbianelli[1], D. Perrone[1,2], and E. Brunesi[3]

[1] University School for Advanced Studies IUSS Pavia
Piazza della Vittoria 15, 27100, Pavia, Italy
giammaria.gabbianelli@iusspavia.it, daniele.perrone@iusspavia.it

[2] Department of Engineering for Innovation, University of Salento
Via per Monteroni, 73100, Lecce, Italy
daniele.perrone@unisalento.it

[3] European Centre for Training and Research in Earthquake Engineering (EUCENTRE)
Via Ferrata 1, 27100, Pavia, Italy
emanuele.brunesi@eucentre.it

Abstract

It is worldwide recognized the importance of assessing the vulnerability of structures in seismic prone zones. Focusing on steel structures, it is well-known that the behavior of beam-to-column connections plays a key role in the seismic response of any moment-resisting frame system. Recently, a research project funded by European Commission investigated the seismic performance of pre-qualified connections through numerical analyses and pseudo-static cyclic testing. From a designer perspective, it is, however, necessary to understand the efficiency of such connections in terms of building performance to take a rational and conscious decision when designing a building. With this in mind, this paper investigates the influence of different beam-to-column connections on the seismic response and vulnerability of medium-rise steel frame structures. The behavior of these structures has been investigated by means of non-linear dynamic analysis for increasing seismic intensity levels using the OpenSeesPy finite element software. The record selection has been carried out through the Average Sa-based method. The building performance has been assessed computing both maximum and residual interstory drifts, as well as fragility curves and absolute acceleration floor response spectra. The last mentioned enables to evaluate the likely damages experienced by acceleration sensitive non-structural elements, giving an additional point-of-view for estimating the building content performance. The outcomes of this study provide useful information for practitioners and designers interested in adopting the new set of pre-qualified connections, clarifying their effects on performance of common buildings and their content.

Keywords: Beam-to-Column Connections, Steel Structures, Seismic Vulnerability, Fragility Curves, Non-structural Elements.

ISSN:2623-3347
Peer-review under responsibility of the organizing committee of COMPDYN 2021.
doi:10.7712/120121.8629.19176

1 INTRODUCTION

The importance of explicit modeling for beam-to-column connections is well-known and recognized in literature with unanimous consensus [1]. The stiffness and strength of beam-of-column connections could affect both the static and dynamic response of structures, leading to unrealistic or unconservative results if their behavior is not adequately considered. To deal with such an issue, experimental data is necessary in order to study the hysteretic response of the connections and to calibrate numerical models that have to be accurate and computationally efficient at the same time. However, analyzing data available in literature, it appears evident that exhaustive test results on the cyclic response of different typologies of beam-column connections are still missing, which could call for further efforts towards standardization.

Following damage observed after the 1994 Northridge (CA, USA) earthquake to steel structures, some significant efforts have been done by US researchers to investigate the response of a wide set of selected joints, commonly adopted in moment-resisting frames (MRFs). The research outcomes allowed to conceive a specific standard [2] that describes criteria for design, detailing, fabrication, and quality of the set of pre-qualified connections.

Regarding the European context, a recent research project [3] tried to fulfill such gaps. The EQUALJOINTS project [3], funded by the European Commission, aimed at providing a qualification of European beam-to-column joints adopted for seismic design. In order to accomplish such a goal, this project selected a set of common joint configurations and focused on the standardization of design and manufacturing procedures. In particular, bolted haunched, bolted extended stiffened end-plate, bolted extended unstiffened end-plate and welded dog-bone joints were experimentally and numerically studied. From the results of the project, it is possible to obtain the cyclic hysteretic response curves, in terms of moment-rotation relationships, which are useful for the explicit modeling of the behavior of connections when integrated in steel MRFs.

Recent studies also focused on the evaluation of the seismic response of steel MRFs considering the influence of joint behavior by means of numerical analyses [4] and shake-table tests [5].

The present study is meant to provide a further contribution on the evaluation of the influence of the explicit modeling of beam-to-column connections in the seismic vulnerability assessment of steel MRFs; in addition, the results of the undertaken nonlinear dynamic analyses are used here to estimate the seismic demand on non-structural elements (NSEs) via floor absolute acceleration spectra [6].

The consideration of NSEs in performance-based earthquake engineering is of paramount importance since they significantly contribute to economic losses and buildings' functionality issues [7-9]. Indeed, recent earthquakes have shown that earthquake-induced direct (i.e., structural and non-structural damages, deaths) and indirect (i.e., downtime and business disruption) losses might be socio-economically arduous [7].

Regarding the seismic performance assessment, several studies dealt with the selection of the most suitable parameter for measuring the damage of steel MRFs due to seismic actions. Generally, the choice bias for the interstory drift [10,11]. Besides, further studies comprised the computation of performance and fragility functions [12-17] or robustness [18] for steel MRFs.

This study aims to evaluate the influence of beam-column connections in the performance of a MRF steel building by employing fragility curves and interstory drift profiles; moreover, for a non-structural perspective, the connections' influence in the seismic demand on NSEs was assessed through acceleration profiles and floor absolute acceleration response spectra.

2 NUMERICAL MODEL OF THE CASE-STUDY BUILDING

The case-study building is a medium-rise steel MRF structure. The structural layout is presented in Figure 1. The building has 6-floor levels, with an interstory height of 3.0 m and a total height of 18 m. In the X-direction, the lateral stability is provided by a 4-bay MRF (Figure 1a) with all the beams spanning 6 m; contrariwise, the lateral support system in the Y direction is offered by diagonal braces (Figure 1b), located in the two end frames (Figure 1c). In this direction, the bay length is equal to 5 m.

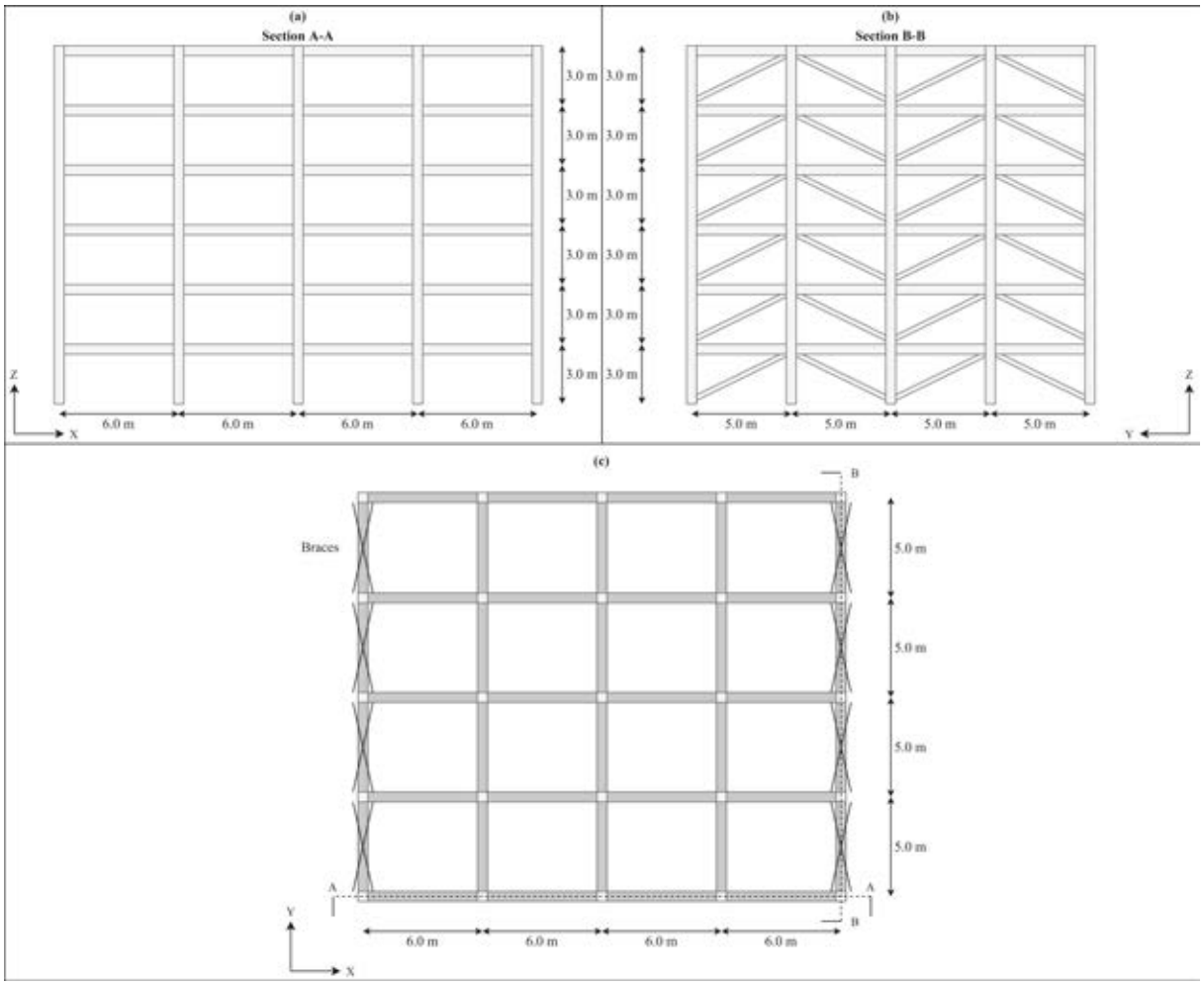

Figure 1: Structural layout: a) moment-resisting frame, b) concentrical braced frame, c) plan-view of the building.

The structure was designed in compliance with European standards [19,20] for steel structures under seismic actions. Table 1 reports the profiles assumed for both beams and columns. It should be noted that all the sections are composed of an S355 material, the behavior of which has been simulated by means of a Menegotto-Pinto material model [21]. The choice of the sections and the bay length in the X-direction was made according to the available data from the experimental tests conducted in [3]. The diagonal braces are composed of hollow square sections with a width of 100 mm and a thickness of 10 mm. Following the load analysis, a uniform load equal to 40.5 kN/m and 30.25 kN/m was applied to the main internal and external beams (parallel to X-direction), respectively. At the roof level, the loads applied to the beams are equal to 33.25 kN/m and 16.78 kN/m for internal and external beams, respectively. Secondary external beams (parallel to Y-direction) are supposed to carry infills' weight,

computed and turned into a uniform load equal to 10 kN/m; the same beams at the roof are instead subjected to a load equal to 0.15 kN/m due to the parapet.

From a numerical point of view, the MRF connections were modeled following two different approaches: 1) full-rigid beam-to-column connections, namely Rigid (R) model and 2) explicit modeling of connections. This latter modeling option makes use of the outcomes of EQUALJOINTS [3], and in particular of results corresponding to the bolted extended stiffened end-plate connections, thus leading to the nomenclature of Extended Stiffened (ES) model. It should be noted that the bolted extended stiffened end-plate joint, in practical design, is generally assumed as rigid; therefore, the comparison between the two modeling approaches is consistent and is meant to shed light into the effects produced by basic modeling assumptions made at the design level. To deal with the geometry of the building, and the selected beams and columns, four connections tested in the EQUALJOINTS project were selected. Using the experimental results, the numerical models simulating the beam-column connections were developed using the pinching4 material model [22] available in OpenSeesPy. For illustrative purposes, and to demonstrate the good prediction capability of the calibrated numerical models, Figure 2 reports the numerical-experimental comparison of the hysteretic curves. Assuming the nomenclature adopted in EQUALJOINTS [3], the joint E1-TB-E-C1 (Figure 2a) and E1-XW-P-C1 (Figure 2a) refer to the HEB280-IPE360 and HEB340-IPE360 connection, respectively.

Floor level	Internal column	External column	Internal beam	External beam	Brace
1	HEB500	HEB340	IPE450	IPE360	100x100x10
2	HEB500	HEB340	IPE450	IPE360	100x100x10
3	HEB340	HEB280	IPE450	IPE360	100x100x10
4	HEB340	HEB280	IPE450	IPE360	100x100x10
5	HEB340	HEB280	IPE450	IPE360	100x100x10
6	HEB340	HEB280	IPE450	IPE360	100x100x10

Table 1: Selected sections for columns, beams, and braces.

The beam-to-column connections in the frames along the Y-direction were modeled as pinned. In this direction, only the braces act as lateral load-bearing elements. These members were modeled as truss elements, i.e., they sustain only tension and compression loads. However, due to their propensity for buckling, the braces were modeled with an asymmetric material, which offers a full-strength for the tension load and a partial-strength for the compression load. It should be noted that the partial strength was calibrated in order to permit the brace to reach its critical load.

The three-dimensional numerical models were developed by the finite-element software OpenSeesPy [23]. Both columns and beams were modeled by force-based beam-column elements with two-point Gauss integration for the interior element and two-point Gauss-Radau integration over each plastic hinge length at the element ends [24]. Such an approach permits to capture the material nonlinearity by discretizing the sections in fibers (about 100 fibers, in this study).

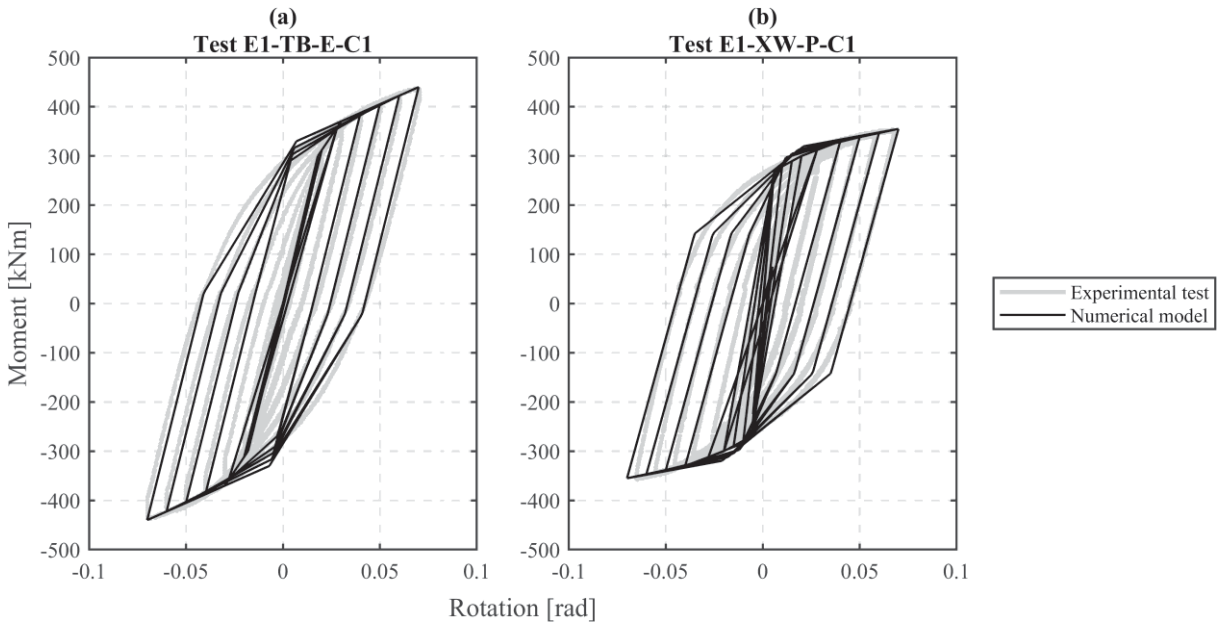

Figure 2: Calibration of the beam-column connection models with the test results provided by EQUALJOINTS [3].

Finally, a modal analysis was performed in order to capture both the free-vibration modes of the building with the two different modeling approaches and obtain essential information for the PSHA and record selection procedure, described in Section 3. Table 2 shows the first six periods of the building obtained from the two modeling approaches. The first, fourth, fifth, and sixth mode are predominantly translational in the X-direction; the second mode is translational in the Y-direction, while the third mode is torsional. Note that these considerations are valid for both R and ES models. As can be observed in Table 2, the actual connections' effect increases the first period by approximately 41%, while minor changes were obtained for the other periods.

Mode	R-model	ES-model	Mode shape
1st	1.24 s	1.75 s	Translational, X-direction
2nd	0.96 s	0.96 s	Translational, Y-direction
3rd	0.71 s	0.77 s	Torsional
4th	0.60 s	0.60 s	Translational, X-direction
5th	0.49 s	0.54 s	Translational, X-direction
6th	0.41 s	0.49 s	Translational, X-direction

Table 2: Free-vibration periods for the R- and ES-model.

In the nonlinear dynamic analyses, a Rayleigh damping model with 2% of critical damping was set for the first and third modes of vibration resulting from each eigenvalue analysis performed.

3 PSHA AND RECORD SELECTION

To obtain a suitable seismic threat for a specific location, a probabilistic seismic hazard analysis (PSHA) should be performed. As it is well-known, the PSHA gives the earthquake rate causing exceedance of any arbitrary ground-motion Intensity Measure (IM) at the site [25]. Therefore, the PSHA provides the seismic actions necessary to perform the structural design and assessment. In this study, the PSHA was performed with the assistance of the

OpenQuake platform [26]. The chosen location to perform the PSHA is the city of L'Aquila, a high seismicity zone in Italy, also tragically known for the catastrophic 2009 earthquake. An average seismic shear-wave velocity from the surface to a depth of 30 m (Vs30) equal to 200 m/s was selected, corresponding to a class soil C in accordance with the soil classification proposed in Eurocode 8 [20]. Note that for the PSHA, an appropriate ground motion prediction equation (GMPE) should be selected; in this study, the GMPE proposed by Lanzano et al. [27] has been used, since such equation is the latest revision for shallow crustal earthquakes in Italy.

Return Period [years]	Probability of Exceedance	Limit state
30	81% in 50 years	SLO – Immediate Occupancy
50	63% in 50 years	SLD – Damage Control Range
475	10% in 50 years	SLV – Life Safety
975	5% in 50 years	SLC – Collapse Prevention
2475	2% in 50 years	
4975	1% in 50 years	

Table 3: Return period of the record selection.

The Multiple-Stripe Analysis (MSA) [28] has been used to perform the seismic vulnerability assessment. Therefore, for each stripe, a PSHA has to be performed, varying the IM increasing the return periods. In Table 3, the six return periods (RPs) selected are reported, together with the probability of exceedance and the limit state associated in accordance with the Italian standard [29].

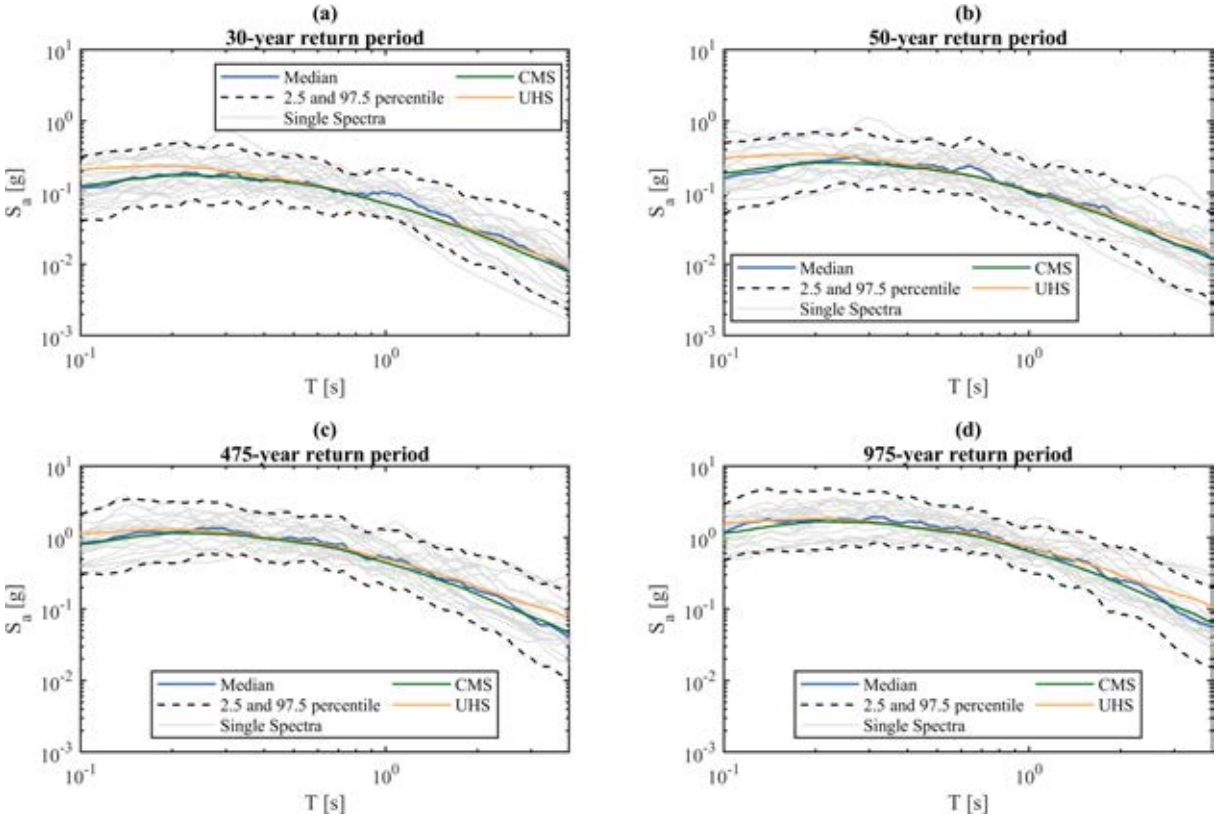

Figure 3: Ground motion spectra for the four selected limit states.

Regarding the choice of the IM and the calculation of the conditional mean spectra (CMS) necessary for the record selection, the average spectral acceleration (AvgSA) was adopted [30]. The AvgSA permits to consider spectral accelerations in a wide range of periods; as suggested by Kohrangi and Bazzurro [30], the calculation of the mean of the log spectral accelerations should be approximately in the range of $0.2T_1$ and $1.5T_1$, where T_1 is the first vibration period of the building. Since in this study there are two models with different first vibration periods, the computation of the range was performed considering the lower first period (1.24s) for the lower bound and the higher first period (1.75s) for the upper bound, leading to a range equal to 0.2s – 2.6s.

For each RP 20 ground motions were selected and, for the return periods associated to the limit state in accordance with the Italian standard [29], depicted in Figure 3 together with Uniform Hazard Spectrum (UHS), the CMS, the median of the selected records, and the median plus/minus the standard deviation, i.e., the 2.5% and 97.5% percentile.

4 STRUCTURAL RESPONSE RESULTS

The MSA is a powerful tool to assess the seismic performance of a structure and, in this case, to investigate the effects of the two considered modeling approaches. The main performance metric considered for steel structures is the interstory drift. Besides, this measure can be discerned in two parts, namely the transient drift and the residual (or permanent) drift. The former one represents the drift experienced during the analysis, and generally, from a performance metric perspective, it corresponds to the maximum drift reached during the whole analysis. Instead, the latter represents the drift in which the structure lies after the dynamic analysis due to permanent deformations caused by the nonlinear behavior of the buckled or yielded components. Therefore, for the sake of completeness, both maximum and residual interstory drifts were recorded.

Moreover, after collecting the accelerations experienced by the case study structures, the floor absolute acceleration response spectra were computed to offer an overview of the differences between the two modeling approaches (R and ES model) in terms of seismic demand on NSEs.

4.1 Interstory drift profiles

The maximum peak interstory drift profiles, for each record, were recorded and are plotted in Figure 4. In particular, Figure 4 shows all the outcomes derived from the six RPs selected and for the two considered configurations. It is worth mentioning that only the results in the X-directions are reported because in the Y-direction pinned connections are assumed. The results in the Y-direction are not discussed also because, from the eigenvalue analysis, it was observed that the different modeling approaches adopted in the two configurations modified the vibration periods but did not affect the global behavior of the structure in terms of modal shapes.

As a general remark, for both R and ES models and for all the RPs, the median peaks drift along the height are concentrated at the fourth and fifth floors. For instance, in the case of life safety limit state (i.e., 475-year RP), the median peak drift occurs at the fourth floor and it is equal to 1.83% for the R model and to 2.61% for the ES model. Similar considerations can be conceived for the other RPs.

As far as the seismic behavior for higher RPs is concerned, both modeling techniques revealed a soft-story mechanism activated between the second and third floors. Therefore, one may deduce that explicit modeling of connections does not change the overall seismic behavior of the structure when subjected to high seismic input.

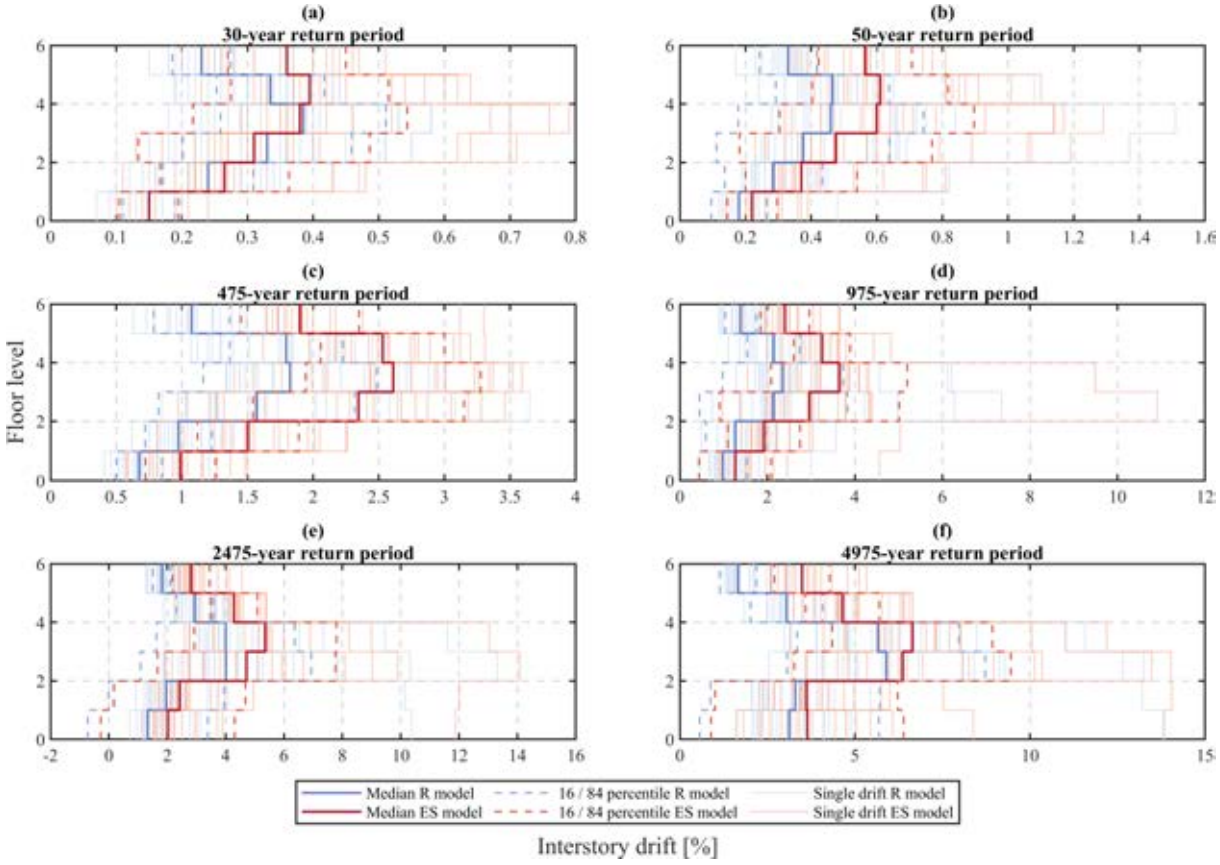

Figure 4: Interstory drift peak profiles for each RP in the X-direction.

However, although the drift trends are quite similar, the inclusion of the actual connections significantly increased the experienced drift values. This is especially true if medium-high RPs are considered. For the 475-year RP an increase of the peak drift equal to 43% is recorded, while for the 975-year RP an increase of 55% is observed. Lower percentage increases of the drifts are instead estimated for the 2475-year and 4975-year RPs, since the experienced drifts present a significant increment of 34% and 17%, respectively. The lower difference of the peak for the two higher RPs (2475-year and 4975-year) is due to the fact that both models, with these RPs, are subjected to large displacements, which induced significant plastic deformation in joints and elements, reducing in turn the stiffness and flattening the dissimilarity between the two structural models. Considering the FEMA-356 [31] interstory drift limitations, the two models behaved quite well. In fact, according to FEMA-356 [31], the maximum drifts are equal to 0.7%, 2.5% and 5% for the immediate occupancy (30-year RP), life safety (475-year RP) and collapse prevention (975-year RP) performance levels, respectively. Only in the case of life safety (Figure 8c) such limits are exceeded since, for the ES model, a maximum peak interstory drift of 2.61% located at the fourth floor is assessed. It is worth mentioning that, although the structure was designed according to EC8 [20], the comparison in terms of maximum interstory drift has been conducted considering the thresholds provided by FEMA-356 [31] because the EC8 [20] only provides some indications for the serviceability limit states.

4.2 Residual drift profiles

The median residual interstory drifts, together with the 16% and 84% percentile and the single drift profiles for each record, are reported in Figure 5. At first glance, it can be noted

that the higher differences between the R and ES models can be appraised for the lower RPs, namely 30- and 50-year RP. In these cases, the increase in terms of residual drifts is around 125% and 280% for the 30- and 50-year RP, respectively. However, considering the first four RPs, it can be noted that the record-to-record variability is considerably higher for the ES model; nevertheless, for the 475- and 975-year RPs, this discrepancy is due to few records with very large residual drift demands.

Overall, both structures behave well with respect to the FEMA-356 [31] limitations. Regarding the immediate occupancy limit state (30-year RP), FEMA-356 [31] indicates a negligible residual drift; in this context, a negligible maximum median value of 0.09% was obtained for the ES model, while an even smaller value was estimated for the R model, i.e., 0.04%. In the case of the life safety limit state (475-year RP), the limitation coincides with 1.0% of residual drift. Again, both models experienced smaller values, i.e., 0.39% and 0.3% for the ES and R models, respectively. Finally, concerning the collapse prevention performance level (975-year RP), a limit of 5% is defined, while the two models did not reach such value, since the maximum median residual drifts corresponded to 0.53% and 0.39% for the ES and R model, respectively.

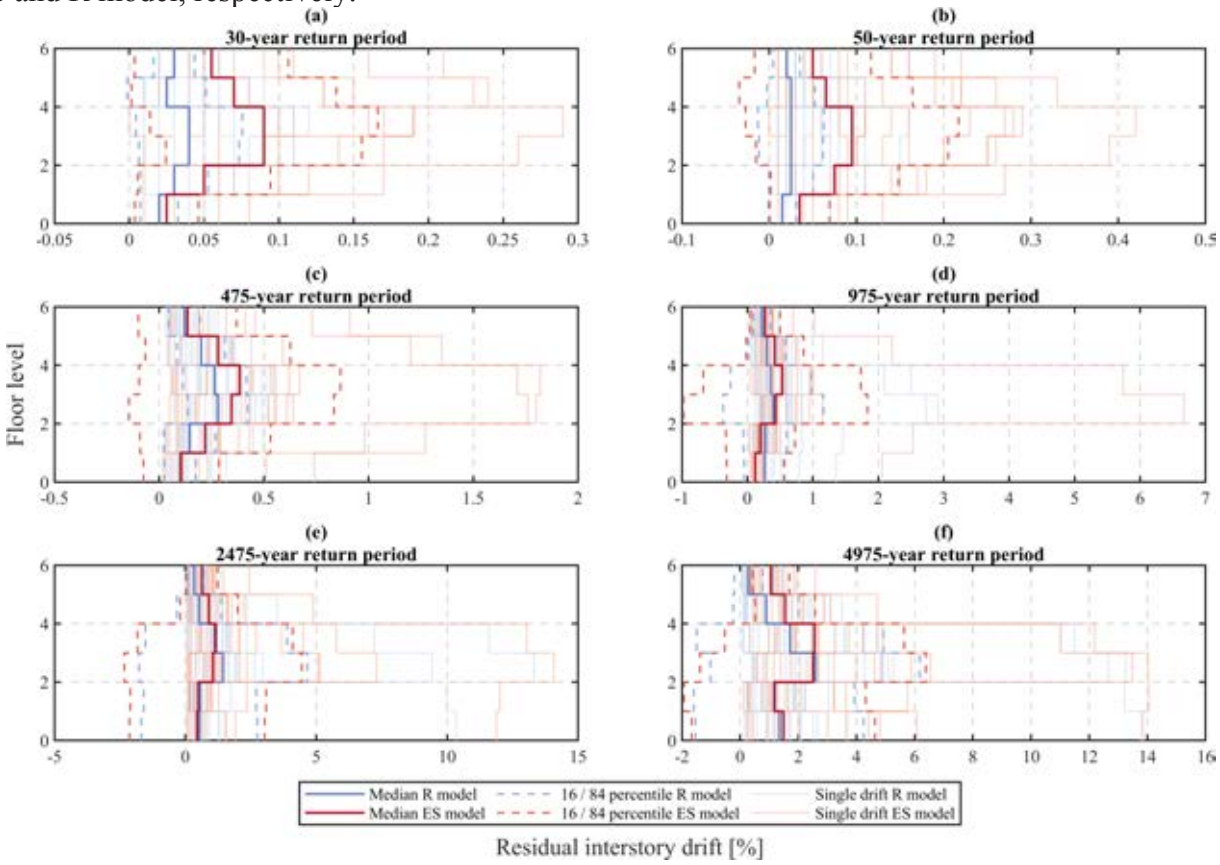

Figure 5: Residual interstory drift peak profiles for each RP in the X-direction.

4.3 Floor acceleration response spectra

Although floor response spectra are generally not considered to assess the structural performance, their evaluation could provide useful information regarding the dynamic response of the building and could also give an insight about the seismic demand at which the NSE installed in the building are prone.

Floor absolute acceleration response spectra were computed for each floor and RP. Figure 6 shows the absolute acceleration floor response spectra related to the roof floor for all the

RPs under investigation. In the first two RPs, namely the 30-year and 50-year RP, distinct peaks can be observed in proximity to the first and fifth (R-model) or sixth (ES-model) free-vibration periods (Figure 6a and 6b). Note that the spectra collected in Figure 6 are related to the X-direction; hence, a peak at the second free-vibration period, which involves masses in Y-direction, is not expected. Considering the differences between the two modeling approaches, it can be inferred that the median peaks in proximity to the sixth and fifth period for the R and ES model reached quite similar values (i.e., 0.8g and 0.66g for the 30-year RP and 1.23g and 1.24g for the 50-year RP, considering the R and ES models, respectively).

As regards the peaks at the first period, the differences are remarkable both in terms of spectral acceleration (0.74g and 0.25g for the 30-year RP and 1.0g and 0.49g for the 50-year RP, referring to R and ES models) and in terms of period shifting. Obviously, the first period elongation was expected for the ES model, as confirmed by the outcomes of the modal analyses performed prior to NLTHAs. For higher RPs, a flattening effect in the first periods can be observed; this phenomenon is quite common and it is due to the nonlinear response of the structures. In all RPs, the absolute acceleration response spectra present significant peaks in proximity to the structures' higher modes. Again, this outcome is not surprising since it is well-known that, in some circumstances, the floor acceleration response spectra are high-mode dominated [32-34]. This behavior is also the consequence of the high fundamental period of the structure, which is associated with lower ground spectral accelerations with respect to the higher modes, although the associated seismic masses are lower.

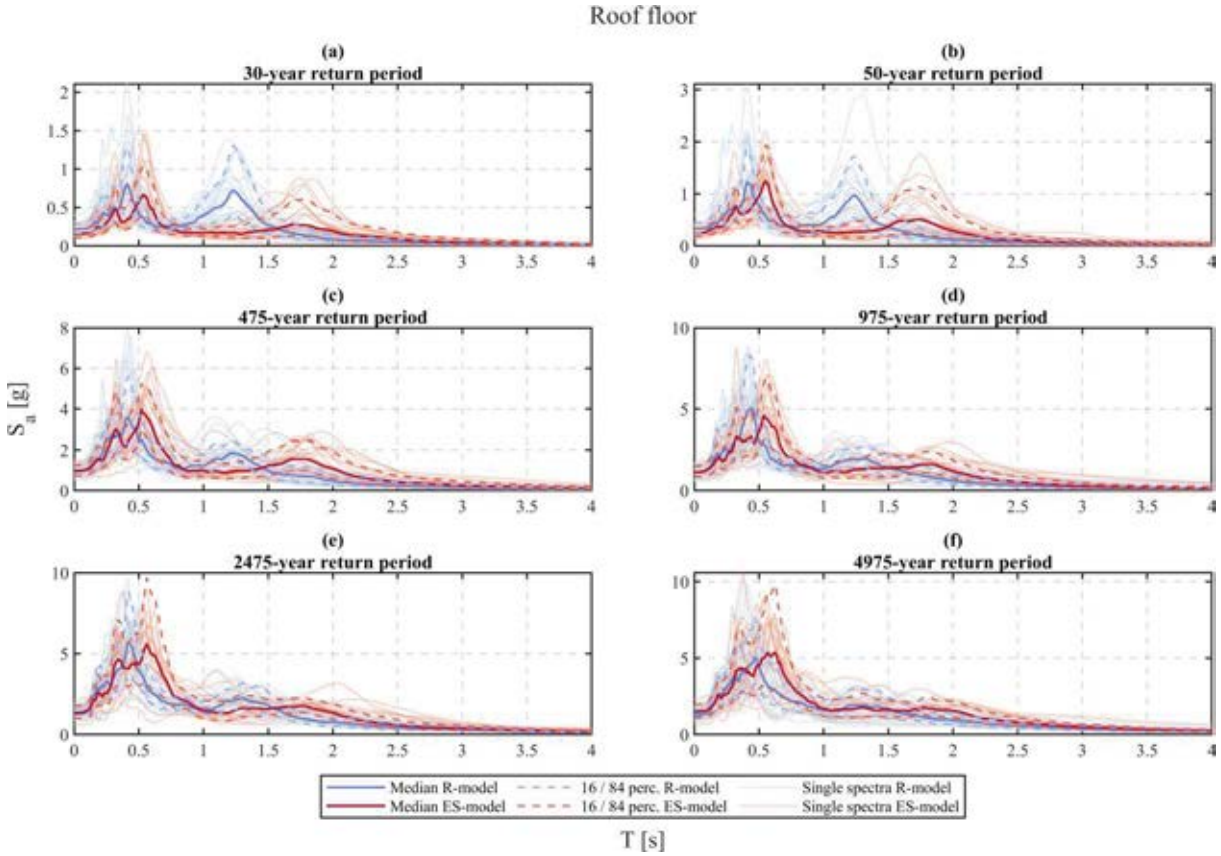

Figure 6: Absolute acceleration floor response spectra at the roof floor for each RP in the X-direction.

5 FRAGILITY CURVES

The calculation of fragility functions was carried out in accordance with the indications provided by Baker [35], in which the fitting technique of the maximum likelihood was suggested. Fragility curves obtained from the NLTHAs are shown in Figure 7; median and dispersion for each curve are also reported.

The limit states were defined following the indications provided by FEMA-356 [31] and already mentioned in the previous sections. FEMA-356 [31], concerning the steel MRFs, suggests adopting a 0.7% transient interstory drift and negligible residual drift for the immediate occupancy limit state; 2.5% transient and 1% residual drift for the life safety limit state and 5% transient or residual drift for the collapse prevention limit state. In addition, a further limit state was considered, namely collapse limit state, in which a limit of 10% transient or residual interstory drift was defined. Therefore, such parameters and thresholds were considered in the fragility curves computation for both models (R and ES model). Note that the curves constructed only refer to the X-direction of the structure.

As can be clearly seen from Figure 7, the ES model (dashed lines) presents a higher seismic vulnerability for most of the limit states. In particular, the median for the attainment of the life safety limit state is equal to 0.34g against a higher value for the R model, i.e., 0.48g. The same applies to the collapse prevention (0.77g versus 0.83g) and collapse (2.06g versus 2.14g) limit states. Only in the case of the immediate occupancy, the median presents identical values (0.09g), although the dispersion is different.

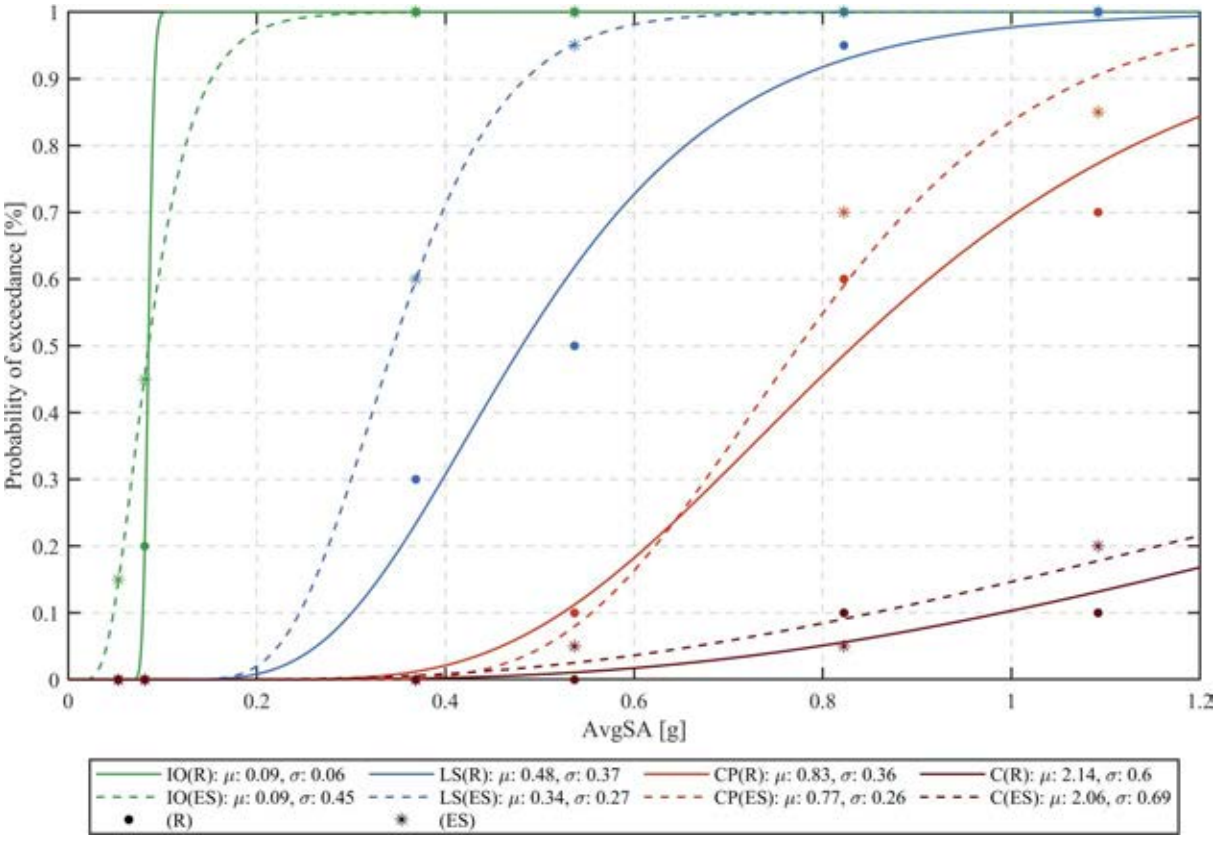

Figure 7: Fragility curves of the case study structure in the X-direction.

A straightforward conclusion can be done from a structural seismic performance perspective, adopting concepts similar to the collapse margin ratio (CMR), i.e. the ratio between the median collapse intensity and the intensity at the collapse limit state. The seismic intensities

(i.e., the AvgSA) for each limit state are 0.05g, 0.37g and 0.54g for the immediate occupancy, life safety and collapse prevention limit states. Therefore, the ratios between the median of each fragility curve and these last intensities are 1.8 (both models) for the immediate occupancy, 1.3 and 0.92 (R and ES model) for the life safety, and 1.54 and 1.43 (R and ES model) for the collapse prevention limit state, respectively. Reflecting the outcomes related to the maximum peak interstory drifts, only in the ES model case for the life safety limit state the ratio fell behind the unity, indicating a dangerous probability of reaching such limit state. This consideration also provides further insights into the importance of an accurate numerical modeling of the beam-column connections.

6 CONCLUSIONS

Past earthquakes demonstrated that, although less attention is generally paid to the seismic performance assessment of steel buildings with respect to, for instance, reinforced concrete and masonry structures, this structural typology could suffer significant damages, both from a structural and non-structural point of view. For this reason, it is of paramount importance to determine suitable models and methods to define the seismic performance correctly. As such, recent researches and projects focused on closing those gaps. In a European context, accurate investigations on pre-qualified joints' seismic behavior for steel buildings were missing until the very last years. Therefore, this study focused on evaluating the influence of the explicit modeling of joints in the structure's seismic performance. The performance metrics considered glanced at both structural and NSEs. Outlining that further research is necessary to define general conclusions for different steel buildings typologies and for all the pre-qualified joints, the outcomes of the analyses conducted in this study are listed in the following:

- The explicit modeling of a rigid joint reduced the structure's overall stiffness; therefore, a significant increment of the interstory drift can be observed. Similar considerations can be made referring to the residual interstory drift.
- The evaluation of the fragility functions, for different performance limit states, pointed out a high vulnerability of the structure if the actual behavior of the joints is explicitly modeled. For the case study structure, only in the case of life safety limit state, for the configuration in which the joints' behavior is modeled, the minimum requirements were not meet.
- The shape of the floor absolute acceleration response spectra is significantly affected by the modeling of the joints, in particular for lower return periods. This consideration is of particular interest because the variation of the periods at which the maximum spectral accelerations are observed could significantly modify demand on and, thus, design of NSEs installed in the structure.

REFERENCES

[1] G. Della Corte, G. De Matteis, R. Landolfo, F.M. Mazzolani, Seismic analysis of MR steel frames based on refined hysteretic models of connections. *Journal of Constructional Steel Research*, **58**, 1331-1345, 2002. https://doi.org/10.1016/S0143-974X(02)00014-7

[2] ANSI/AISC 358, *Prequalified Connections for Special and Intermediate Steel Moment Frames for Seismic Applications, including Supplements No. 1 (2018) and No. 2 (2020)*. American Institute of Steel Construction (AISC), CHICAGO, IL, 60601, 2016.

[3] R. Landolfo et al., European pre-qualified steel joints (EQUALJOINTS). *Research fund for coal and steel (RFCS)*, Grant agreement RFSR-CT-2013-00021, 2013-2016.

[4] S. Costanzo, M. D'Aniello, R. Landolfo, The influence of moment resisting beam-to-column connections on seismic behavior of chevron concentrically braced frames. *Soil Dynamics and Earthquake Engineering*, **113**, 136-147, 2018. https://doi.org/10.1016/j.soildyn.2018.06.001

[5] R. Tartaglia, M. D'Aniello, R. Landolfo, Numerical simulations to predict the seismic performance of a 2-story steel moment-resisting frame. *Materials*, **13**, 4831, 2020. https://doi.org/10.3390/ma13214831

[6] I. González, A. Silva, L. Macedo, R. Monteiro, J.M. Castro, Critical assessment of estimation procedures for floor acceleration demands in steel moment-resisting frames. *Frontiers in Built Environment*, **5:139**, 2019. https://doi.org/10.3389/fbuil.2019.00139

[7] A. Silva, L. Macedo, R. Monteiro, J.M. Castro, Earthquake-induced loss assessment of steel buildings designed to Eurocode 8. *Engineering Structures*, **208**, 110244, 2020. https://doi.org/10.1016/j.engstruct.2020.110244

[8] G. Cantisani, G. Della Corte, T.J. Sullivan, R. Roldan, Displacement-based simplified seismic loss assessment of steel buildings. *Journal of Earthquake Engineering*, **24:sup1**, 146-178, 2020. https://doi.org/10.1080/13632469.2020.1713932

[9] A. Silva, J.M. Castro, R. Monteiro, Brace-to-frame connection modelling effects on seismic loss assessment of steel concentrically-braced frames. *Journal of Constructional Steel Research*, **172**, 106230, 2020. https://doi.org/10.1016/j.jcsr.2020.106230

[10] A. Gupta, H. Krawinkler, Estimation of seismic drift demands for frame structures. *Earthquake Engineering and Structural Dynamics*, **29**, 1287-1305, 2000. https://doi.org/10.1002/1096-9845(200009)29:9<1287::AID-EQE971>3.0.CO;2-B

[11] J. Ruiz-García, J.C. Negrete-Manriquez, Evaluation of drift demands in existing steel frames under as-recorded far-field and near-fault mainshock-aftershock seismic sequences. *Engineering Structures*, **33(2)**, 621-634, 2011. https://doi.org/10.1016/j.engstruct.2010.11.021

[12] R.J. Merino Vela, E. Brunesi, R. Nascimbene, Seismic assessment of an industrial frame-tank system: development of fragility functions. *Bulletin of Earthquake Engineering*, **17(5)**, 2569-2602, 2019. https://doi.org/10.1007/s10518-018-00548-2

[13] E. Brunesi, R. Nascimbene, G.A. Rassati, Seismic fragility analysis of MRFs with PR bolted connections using IDA approach. *Key Engineering Materials*, **763**, 678-685, 2018. https://doi.org/10.4028/www.scientific.net/KEM.763.678

[14] F. Gutiérrez-Urzua, F. Freddi, L. Di Sarno, Comparative analysis of code-based approaches for seismic assessment of existing steel moment resisting frames, *Journal of Constructional Steel Research*, **181**, 106589, 2021. https://doi.org/10.1016/j.jcsr.2021.106589

[15] G. Gabbianelli, F. Cavalieri, R. Nascimbene, Seismic vulnerability assessment of steel storage pallet racks, *Ingegneria Sismica*, **37(2)**, 18-40, 2020.

[16] A. Silva, Y. Jiang, L. Macedo, J.M. Castro, R. Monteiro, N. Silvestre, Seismic performance of composite moment-resisting frames achieved with sustainable CFST members. *Frontiers of Structural and Civil Engineering*, **10(3)**, 312-332, 2016. https://doi.org/10.1007/s11709-016-0345-y

[17] A. Silva, Y. Jiang, L. Macedo, J.M. Castro, R. Monteiro, N. Silvestre, Monotonic and cyclic flexural behaviour of square/rectangular rubberized concrete-filled steel tubes. *Journal of Constructional Steel Research*, **139**, 385-396, 2017. https://doi.org/10.1016/j.jcsr.2017.09.006

[18] D. Rodríguez, E. Brunesi, R. Nascimbene, Fragility and sensitivity analysis of steel frames with bolted-angle connections under progressive collapse. *Engineering Structures*, **228**, 111508, 2021. https://doi.org/10.1016/j.engstruct.2020.111508

[19] EN 1993-1-1, *Eurocode 3: Design of steel structures - Part 1-1: General rules and rules for buildings*. European Committee for Standardisation, Brussels, Belgium, 2014.

[20] E N 1998-1, *Eurocode 8: Design of structures for earthquake resistance - Part 1: General rules, seismic actions and rules for buildings*. European Committee for Standardisation, Brussels, Belgium, 2011.

[21] K. Kolozvari, K. Orakcal, J. W. Wallace, *Shear-flexure interaction modeling for reinforced concrete structural walls and columns under reversed cyclic loading, PEER 2015/12*. Pacific Earthquake Engineering Research Center, 2015.

[22] L.N. Lowes, N. Mitra, A. Altoontash, *A beam-column joint model for simulating the earthquake response of reinforced concrete frames, PEER 2003/10*. Pacific Earthquake Engineering Research Center, 2004.

[23] M. Zhu, F. McKenna, M.H. Scott, OpenSeesPy: Python library for the OpenSees finite element framework. *SoftwareX*, **7**, 6-11, 2018. https://doi.org/10.1016/j.softx.2017.10.009

[24] M.H. Scott, G.L. Fenves, Plastic hinge integration methods for force-based beam-column elements. *Journal of Structural Engineering*, **132(2)**, 244-252, 2006. https://doi.org/10.1061/(ASCE)0733-9445(2006)132:2(244)

[25] C.A. Cornell, Engineering seismic risk analysis. *Bulletin of the Seismological Society of America*, **58(5)**, 1583-1606, 1968.

[26] M. Pagani, D. Monelli, G. Weatherill, L. Danciu, H. Crowley, V. Silva, P. Henshaw, L. Butler, M. Nastasi, L. Panzeri, M. Simionato, D. Vigano, OpenQuake Engine: An Open Hazard (and Risk) Software for the Global Earthquake Model. *Seismological Research Letters*, **85(3)**, 692-702, 2014. https://doi.org/10.1785/0220130087

[27] G. Lanzano, L. Luzi, F. Pacor, C. Felicetta, R. Puglia, S. Sgobba, M. D'Amico, A revised ground-motion prediction model for shallow crustal earthquakes in Italy, Bulletin of Seismological Society of America, **109(2)**, 525-540, 2019. https://doi.org/10.1785/0120180210

[28] F. Jalayer, C.A. Cornell, Alternative non-linear demand estimation methods for probability-based seismic assessments, *Earthquake Engineering and Structural Dynamics*, **38(8)**, 951-972, 2009. https://doi.org/10.1002/eqe.876

[29] NTC18, *Norme Tecniche per le Costruzioni, DM 17/1/2018*. Gazzetta Ufficiale della Repubblica Italiana, Italian Ministry of Infrastructure and Transport, Rome, Italy, 2018.

[30] M. Kohrangi, P. Bazzurro, D. Vamvatsikos, A. Spillatura, Conditional spectrum-based ground motion record selection using average spectral acceleration, *Earthquake Engineering and Structural Dynamics*, **46(10)**, 1667-1685, 2017. https://doi.org/10.1002/eqe.2876

[31] FEMA-356, *Prestandard and commentary for the seismic rehabilitation of buildings*. Federal Emergency Management Agency, Washington, DC 20472, 2000.

[32] G. Gabbianelli, D. Perrone, E. Brunesi, R. Monteiro, Seismic acceleration and displacement demand profiles of non-structural elements in hospital buildings, *Buildings*, **10(12)**, 243, 1-19, 2020. https://doi.org/10.3390/buildings10120243

[33] V. Vukobratović, S. Ruggieri, Floor acceleration demands in a twelve-storey RC shear wall building, *Buildings*, **11(2)**, 38, 1-20, 2021. https://doi.org/10.3390/buildings11020038

[34] R. Merino, D. Perrone, A. Filiatrault, Consistent floor response spectra for performance-based seismic design of non-structural elements, *Earthquake Engineering and Structural Dynamics*, **49(3)**, 261-284, 2021. https://doi.org/10.1002/eqe.3236

[35] J.W. Baker, Efficient analytical fragility function fitting using dynamic structural analysis, *Earthquake Spectra*, **31(1)**, 579-599, 2015. https://doi.org/10.1193/021113EQS025M